RESEARCH ARTICLE

Key Points:
- To identify the key parameters of the PT-JPL model specific to different biomes by using SA with forcing data
- To optimize the selected key parameters using the DEMC scheme for different biomes
- To evaluate and compare the performance of the original model and the optimized model across different biomes

Parameter sensitivity analysis and optimization for a satellite-based evapotranspiration model across multiple sites using Moderate Resolution Imaging Spectroradiometer and flux data

Kun Zhang[1,2] (ID)**, Jinzhu Ma[1,2], Gaofeng Zhu[1,2], Ting Ma[1,2], Tuo Han[1,2], and Li Li Feng[1,2]**

[1]Key Laboratory of Western China's Environmental Systems (Ministry of Education), Lanzhou University, Lanzhou, China, [2]College of Earth and Environmental Sciences, Lanzhou University, Lanzhou, China

Abstract Global and regional estimates of daily evapotranspiration are essential to our understanding of the hydrologic cycle and climate change. In this study, we selected the radiation-based Priestly-Taylor Jet Propulsion Laboratory (PT-JPL) model and assessed it at a daily time scale by using 44 flux towers. These towers distributed in a wide range of ecological systems: croplands, deciduous broadleaf forest, evergreen broadleaf forest, evergreen needleleaf forest, grasslands, mixed forests, savannas, and shrublands. A regional land surface evapotranspiration model with a relatively simple structure, the PT-JPL model largely uses ecophysiologically-based formulation and parameters to relate potential evapotranspiration to actual evapotranspiration. The results using the original model indicate that the model always overestimates evapotranspiration in arid regions. This likely results from the misrepresentation of water limitation and energy partition in the model. By analyzing physiological processes and determining the sensitive parameters, we identified a series of parameter sets that can increase model performance. The model with optimized parameters showed better performance ($R^2 = 0.2$–0.87; Nash-Sutcliffe efficiency (NSE) = 0.1–0.87) at each site than the original model ($R^2 = 0.19$–0.87; NSE = -12.14–0.85). The results of the optimization indicated that the parameter β (water control of soil evaporation) was much lower in arid regions than in relatively humid regions. Furthermore, the optimized value of parameter m_1 (plant control of canopy transpiration) was mostly between 1 to 1.3, slightly lower than the original value. Also, the optimized parameter T_{opt} correlated well to the actual environmental temperature at each site. We suggest that using optimized parameters with the PT-JPL model could provide an efficient way to improve the model performance.

1. Introduction

Evapotranspiration (ET) is an important land surface process in climatology and a nexus of the terrestrial water, energy, and carbon cycles [*Jung et al.*, 2010; *Senay et al.*, 2011; *Wang and Dickinson*, 2012]. About 60% of annual land precipitation is returned to the atmosphere through the ET process [*Baumgartner and Reichel*, 1975; *Chahine*, 1992; *Oki and Kanae*, 2006], and the associated latent heat of vaporization consumes more than 50% of the absorbed net solar radiation [*Trenberth and Smith*, 2009; *Vinukollu et al.*, 2011]. Thus, accurately estimating the spatial distribution and temporal behavior of ET is important for environmental simulation, climate change research, and irrigation and water resource management [*Rango and Shalaby*, 1998; *Raupach*, 2001; *Keane et al.*, 2002; *Dodds et al.*, 2005].

Fortunately, remote sensing data sets offer an opportunity for mapping the spatial distribution of ET at scales ranging from regional to global [*AghaKouchak et al.*, 2015]. Remote sensing-based ET estimation methods fall into two broad categories: (1) empirical/statistical methods that relate ET to some easily obtained satellite-derived variables (e.g., radiation, land surface temperature, and vegetation index) and (2) process-based methods, which estimate ET on the basis of the Penman-Monteith equation [*Monteith*, 1965; *Cleugh et al.*, 2007; *Mu et al.*, 2007, 2011], the Priestley-Taylor approach [*Priestley and Taylor*, 1972; *Fisher et al.*, 2008], or the residual method of the energy balance equation [*Bastiaanssen et al.*, 1998; *Su*, 2002; *Norman et al.*, 1995]. Among them, the Priestly-Taylor Jet Propulsion Laboratory (PT-JPL) model proposed by *Fisher et al.* [2008] has been widely used to estimate ET because of its minimal requirements for ground-based measurements and its good performance [*Feng et al.*, 2015; *Michel et al.*, 2016; *Zhu et al.*, 2016]. For example, *Ershadi et al.* [2014] illustrated that the PT-JPL model provided the best results among four commonly used ET

models across 20 flux towers. Using 45 globally distributed flux towers, *McCabe et al*. [2016] also reported that the PT-JPL model provided the best statistical performance among four remote sensing-based ET models.

Nevertheless, there are deficiencies in the application of the PT-JPL model. The PT-JPL model is highly complex with many ecophysiological parameters, which may vary with the environmental conditions, plant functional types (PFTs), and other factors [*Zhu et al*., 2016]. Thus, there is a need to identify the parameters in the PT-JPL model that do or do not have significant influence on model simulations across different biomes and environmental conditions. The parameter sensitivity analysis (SA) method is capable of playing this role in identifying sensitive parameters and can help concentrate efforts on model calibration and optimization [*Saltelli et al*., 2000; *Wagener et al*., 2003]. Also, based on SA, the robustness of the model can be analyzed for future modification and improvement [*Fraedrich and Goldberg*, 2000; *Confalonieri et al*., 2010]. In previous studies, the parameter SA algorithm has been applied mainly to complex hydrological, ecological, crop, and environmental models [*Pappenberger et al*., 2008; *van Werkhoven et al*., 2008; *Yang*, 2011; *Nossent et al*., 2011; *Fu et al*., 2012; *Zhang et al*., 2013]. Using the PT-JPL model, *Garcia et al*. [2013] conducted a SA for all the variables (including the forcing data and constant parameters) at only two arid sites (Sahelian savanna and Mediterranean grasslands). To obtain more accurate data, the SA in the PT-JPL model should be applied across a wider range of biomes and environmental conditions.

Previous studies have demonstrated that the Bayesian approach, such as Markov chain Monte Carlo (MCMC), provides powerful new tools for optimizing model parameters and quantifying the influence of uncertainties [*Clark and Gelfand*, 2006; *Zhu et al*., 2013, 2014]. However, MCMC-based approaches often suffer from problems related to proper initialization and proposal density function, which may prevent the algorithm from efficiently reaching convergence [*Haario et al*., 2006]. Alternatively, the Differential Evolution Markov Chain (DE-MC) algorithm [*Ter Braak*, 2006] is designed for global optimization in real parameter spaces by combining the differential evolution algorithm of *Price and Storn* [1997]. Compared to the MCMC-based approaches, the DE-MC algorithm is more suitable to draw inference on high-dimensional models [*Ter Braak*, 2006]. However, limited studies have been conducted by using the DE-MC approach to optimize the remote sensing-based ET models.

In this paper, we used the Moderate Resolution Imaging Spectroradiometer (MODIS) products (MOD13Q1) and flux data from 44 eddy covariance flux towers located throughout the world as the forcing data. These sites represent typical PFTs. The purpose of this work is (1) to identify the key parameters of the PT-JPL model specific to different biomes and climate conditions by using SA with forcing data based on eddy flux data and MODIS products and (2) to optimize the selected sensitive parameters using the DE-MC scheme for different PFTs and climatic conditions.

2. Data

To identify the sensitive parameters and evaluate the performance of the PT-JPL model across different biomes, we used observed data from 44 flux sites (Figure 1 and Table 1), that included 41 sites from the FLUXNET [*Baldocchi et al*., 2001; *Jung et al*., 2011] and three sites from the Coordinated Enhanced Observation Network of China [*Liu et al*., 2011]. These sites extend across four continents (Asia, Oceania, North America, and South America) and represent eight typical PFTs that follows the International Geosphere–Biosphere Programme classification: grasslands (five sites), croplands (five sites), savannas and woody savannas (SA, nine sites), shrublands (seven sites), deciduous broadleaf forest (DBF, five sites), evergreen broadleaf forest (EBF, two sites), evergreen needleleaf forest (ENF, five sites), and mixed forest (MF, six sites). The data used in the analysis are all available as the so-called "Level 2 and Level 3 with gaps" files at the data repository. The only adjustments made to these data were as follows: (i) if the measured energy imbalance (net radiation minus latent, sensible, and ground heat flux) exceeds $300 \, \text{W} \cdot \text{m}^{-2}$, the fluxes for that half hour were treated as missing, (ii) if data gaps were less than 6 h in length, the missing data were estimated by using the linear interpolation method, and (iii) any day after interpolation which did not have a complete diurnal cycle of necessary measurements for model evaluations was not used in the analysis. After these adjustments, the energy balance closure (the sum of sensible and latent heat flux against available energy) across the selected sites ranges from 71% to 95% with a mean of 82.5%, and the intercept values range -11.6–$22.8 \, \text{W} \cdot \text{m}^{-2}$ with a mean of $4.18 \pm 8.51 \, \text{W} \cdot \text{m}^{-2}$ (see details in supporting information). Thus, the data quality at the selected sites was relatively high and suitable for the purposes of model performance
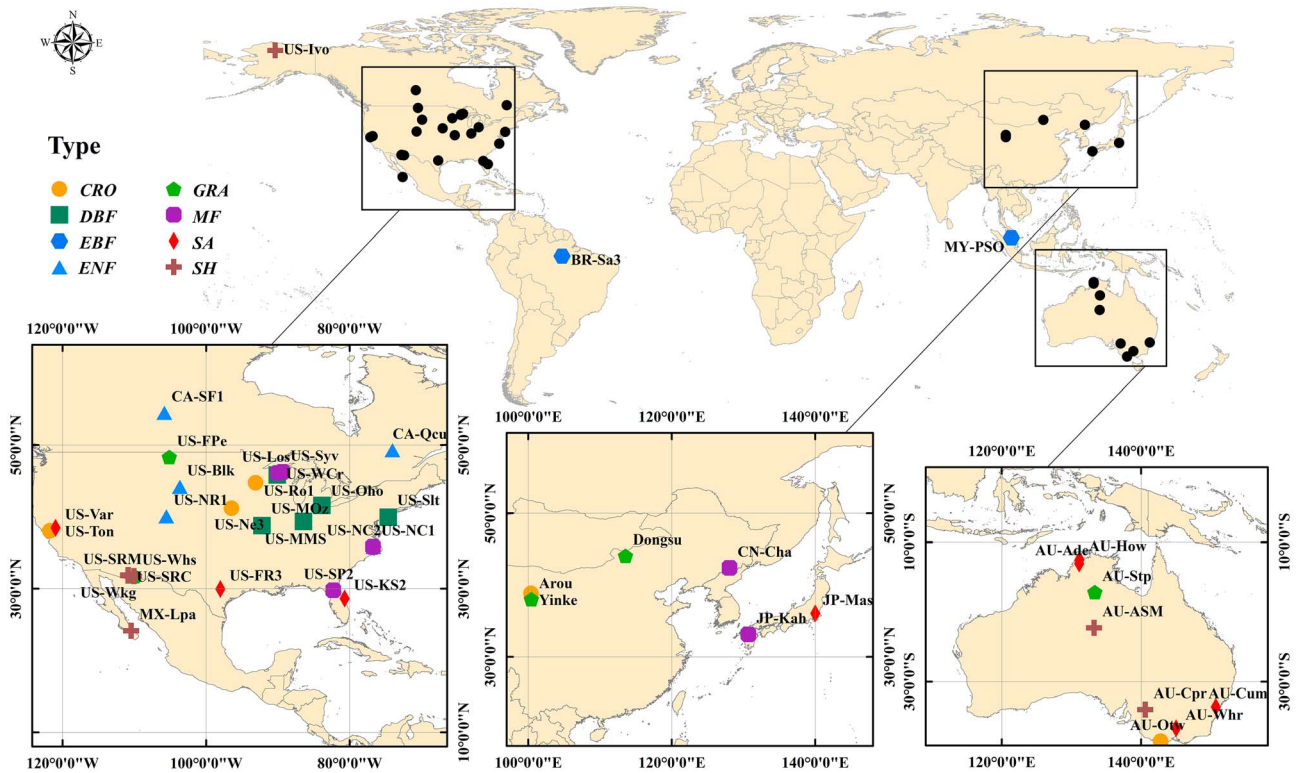
Figure 1. Flux sites used in the study. Ecosystems are identified with the International Geosphere-Biosphere Programme.

evaluations. To account for the biased low latent heat flux measurements due to the energy imbalance at our selected sites (5%–19%), the directly measured latent heat fluxes were also corrected by using the residual energy balance method and the Bowen ratio method [*Twine et al.*, 2000; *Jung et al.*, 2010] (supporting information). In our prior test study, the model performances were evaluated against both the directly observed and the corrected latent heat fluxes. It was found that the within-site temporal variations of the observed (corrected) latent heat flux were well captured by the model, and its performances become better at some sites (a total of 12 sites) when evaluating against the corrected latent heat fluxes in comparison with that against the directly observed latent heat flux data. However, at some sites (especially at the arid regions) the model performances are not satisfactory regardless of evaluating against the directly observed or the corrected latent heat flux data. Thus, the uncertainty in model parameters may be a main source of the disagreements between observed and simulated latent heat fluxes.

We acquired both the normalized difference vegetation index (NDVI) and the enhanced vegetation index (EVI) from MODIS products (MOD13Q1, http://modis.gsfc.nasa.gov/). It can provide a 16 day composite image with a spatial resolution of 250 m.

3. Model and Methods

3.1. PT-JPL Model

The Priestley-Taylor (PT) [*Priestley and Taylor*, 1972] equation is a simplified, but successful model for estimating the potential evapotranspiration (PET) from wet surfaces. Using a series of indicators based on atmospheric and ecophysiological constraints, *Fisher et al.* [2008] proposed the PT-JPL model to downscale the PET to actual evapotranspiration. In the PT-JPL model the total ET is partitioned into canopy transpiration (LE_c), soil evaporation (LE_s), and interception evaporation (LE_i). These are defined as

$$LE_c = (1 - f_{\text{wet}})f_g f_t f_m \alpha \frac{\Delta}{\Delta + \gamma} R_{nc} \tag{1}$$

Table 1. Main Characteristics of Selected Sites[a]

Site ID		Country	Lat	Lon	Elevation	Climate	P	T	Year	L	Source	References
Croplands												
S1	AU-Otw	Australia	−38.53	142.82	54	Cfb	800	13.8	2008–2010	3	OzFlux	*Jung et al.* [2009]
S2	US-Ne3	USA	41.18	−96.44	363	Dfa	783	10.1	2009–2011	2	AmeriFlux	*Ershadi et al.* [2014]
S3	US-Ro1	USA	44.71	−93.09	290	Dfa	879	6.4	2010–2012	2	AmeriFlux	*Xue and Pan* [2008]
S4	US-Snd	USA	38.04	−121.75	−5	Csb	358	15.6	2012–2014	2	AmeriFlux	*Ryu et al.* [2012]
S5	Yingke	China	38.86	100.41	1519	Bwk	130	7.3	2008–2009	2	RCE-TEA	*Li et al.* [2009]
Deciduous Broadleaf Forest												
S6	US-MMS	USA	39.32	−86.41	275	Cfa	1032	10.9	2012–2014	2	AmeriFlux	*Fu et al.* [2014]
S7	US-MOz	USA	38.74	−92.2	219.4	Cfa	986	12.1	2011–2013	2	AmeriFlux	*Ershadi et al.* [2014]
S8	US-Oho	USA	41.55	−83.84	230	Dfa	849	10.1	2009–2011	2	AmeriFlux	*Stoy et al.* [2014]
S9	US-Slt	USA	39.91	−74.6	30	Dfa	1138	11	2010–2012	2	AmeriFlux	*Hollinger et al.* [2010]
S10	US-WCr	USA	45.81	−90.08	520	Dfb	787	4	2012–2014	2	AmeriFlux	*Stoy et al.* [2014]
Evergreen Broadleaf Forest												
S11	BR-Sa3	Brazil	−3.02	−54.97	100	Am	2043	26.1	2002–2004	2	AmeriFlux	*Stoy et al.* [2014]
S12	MY-PSO	Malaysia	2.97	102.31	75	Af	1865	25.3	2007–2009	2	AsiaFlux	*Kamakura et al.* [2011]
Evergreen Needleleaf Forest												
S13	CA-Qcu	Canada	49.27	−74.04	392.3	Dfc	950	0.1	2008–2010	2	AmeriFlux	*Stoy et al.* [2014]
S14	CA-SF1	Canada	54.49	−105.82	536	Dfc	470	0.4	2004–2006	2	AmeriFlux	*Stoy et al.* [2014]
S15	US-Blk	USA	44.16	−103.65	1718	Dfb	574	6.2	2006–2008	2	AmeriFlux	*Xue and Pan* [2008]
S16	US-NC2	USA	35.8	−76.67	5	Cfa	1320	16.6	2006–2008	2	AmeriFlux	*Stoy et al.* [2013]
S17	US-NR1	USA	40.03	−105.55	3050	Dfc	800	1.5	2011–2013	2	AmeriFlux	*Stoy et al.* [2013]
Grasslands												
S18	Arou	China	38.04	100.46	3033	ET	396	0.7	2008–2009	2	RCE-TEA	*Zhu et al.* [2013, 2014]
S19	AU-Stp	Australia	−17.15	133.35	250	Bsh	640	25.8	2014–2015	3	OzFlux	*Beringer et al.* [2016]
S20	Dongsu	China	44.09	113.57	970	Bwk	287	3.8	2008–2009	2	RCE-TEA	*Zhu et al.* [2013, 2014]
S21	US-FPe	USA	48.31	−105.1	634	BSk	335	5.5	2006–2008	2	AmeriFlux	*Stoy et al.* [2013]
S22	US-Wkg	USA	31.74	−109.94	1531	BSk	407	15.6	2012–2014	2	AmeriFlux	*Stoy et al.* [2013]
Mixed Forests												
S23	CN-Cha	China	42.4	128.1	731	Dwb	713	3.6	2004–2005	2	AsiaFlux	*Stoy et al.* [2013]
S24	JP-Kah	Japan	33.13	130.71	165	Cfa	2037	14.7	2006–2008	2	AsiaFlux	*Shimizu* [2007]
S25	US-Los	USA	46.08	−89.98	480	Dfb	828	4.1	2006–2008	2	AmeriFlux	*Stoy et al.* [2013]
S26	US-NC1	USA	35.81	−76.71	5	Cfa	1320	16.6	2007–2009	2	AmeriFlux	*Stoy et al.* [2013]
S27	US-SP2	USA	29.76	−82.24	50	Cfa	1314	20.1	2007–2009	2	AmeriFlux	*Stoy et al.* [2013]
S28	US-Syv	USA	46.24	−89.35	540	Dfb	826	3.81	2005–2007	2	AmeriFlux	*Stoy et al.* [2013]
Savannas/Woody Savannas												
S29	AU-Ade	Australia	-13.08	131.12	90	Aw	1730	27.4	2007–2009	3	OzFlux	*Beringer et al.* [2016]
S30	AU-Cum	Australia	-33.61	150.72	200	Cfa	800	18.5	2013–2015	3	OzFlux	*Beringer et al.* [2016]
S31	AU-How	Australia	-12.49	131.15	64	Aw	1750	27	2013–2015	3	OzFlux	*Beringer et al.* [2016]
S32	AU-Whr	Australia	-36.67	145.03	165	Cfb	558	15	2013–2015	3	OzFlux	*Beringer et al.* [2016]
S33	JP-Mas	Japan	36.05	140.03	12	Cfa	1389	14.6	2003–2005	2	AsiaFlux	*Ryu et al.* [2012]
S34	US-FR3	USA	29.94	−97.99	232	Cfa	869	19.6	2010–2012	2	AmeriFlux	*Heinsch et al.* [2004]
S35	US-KS2	USA	28.61	−80.67	3	Cwa	1294	21.7	2004–2006	2	AmeriFlux	*Stoy et al.* [2013]
S36	US-Ton	USA	38.43	−120.97	177	Csa	559	15.8	2012–2014	2	AmeriFlux	*Stoy et al.* [2014]
S37	US-Var	USA	38.41	−120.95	129	Csa	559	15.8	2012–2014	2	AmeriFlux	*Stoy et al.* [2013]
Shrublands												
S38	AU-ASM	Australia	−22.28	133.25	606	Bsh	306	21	2011–2013	3	OzFlux	*Beringer et al.* [2016]
S39	AU-Cpr	Australia	−34	140.59	32	Bsk	240	17.3	2012–2014	3	OzFlux	*Meyer et al.* [2015]
S40	MX-Lpa	Mexico	24.13	−110.44	21	Bwh	182	23.6	2006–2008	2	AmeriFlux	*Bell et al.* [2012]
S41	US-Ivo	USA	68.49	−155.75	568	ET	304	-8.3	2005–2007	2	AmeriFlux	*Wang et al.* [2010]
S42	US-SRC	USA	3144.91	−110.84	991	Bsk	310	20	2010–2012	2	AmeriFlux	*Bunting et al.* [2014]
S43	US-SRM	USA	31.82	−110.87	1120	Bsk	380	17.9	2012–2014	2	AmeriFlux	*Scott et al.* [2009]
S44	US-Whs	USA	31.74	−110.05	1370	Bsk	320	17.6	2012–2014	2	AmeriFlux	*Wang et al.* [2010]

[a]P and T represent the annual precipitation (mm) and average temperature (°C), respectively. Climate represents the Koppen Climate Classification and L is the processing level of data.

$$LE_s = (f_{\text{wet}} + f_{\text{sm}}(1 - f_{\text{wet}}))\alpha \frac{\Delta}{\Delta + \gamma}(R_{\text{ns}} - G) \qquad (2)$$

$$LE_i = f_{\text{wet}}\alpha \frac{\Delta}{\Delta + \gamma}R_{\text{nc}} \qquad (3)$$

Table 2. Parameters and Prior Ranges of the PT-JPL Model

Name	Intervening Variable	Initial Value	References	Prior Range	References
m_1	$f_{APAR} f_m f_g$	1.2×1.136	*Gao and Li* [2000]; *Huete et al.* [2002]	$[0, \min\{m_2 NDVI + b_2 - b_1\}]$	This study
b_1	$f_{APAR} f_m f_g$	$1.2 \times (-0.04)$	*Gao and Li* [2000]; *Huete et al.* [2002]	$[-0.039, -0.025]$	*Garcia et al.* [2013]
m_2	$f_{IPAR} f_g$ LAI	1	*Fisher et al.* [2008]	$[0.9, 1.1]$	*Yao et al.* [2013]
b_2	$f_{IPAR} f_g$ LAI	-0.05	*Fisher et al.* [2008]	$[-0.06, -0.04]$	*Garcia et al.* [2013]
T_{opt}	f_t	25	*Garcia et al.* [2013]; *Yao et al.* [2014]	$[5, 40]$	This study
β	f_{sm}	1	*Fisher et al.* [2008]	$[0, 1]$	This study
k_{Rn}	R_{ns}	0.6	*Impens and Lemeur* [1969]	$[0.3, 0.6]$	*Garcia et al.* [2013]
k_{PAR}	LAI	0.5	*Ross* [1976]	$[0.3, 0.6]$	*Garcia et al.* [2013]

where f_{wet} is the relative surface wetness (unitless), f_g is the green canopy fraction (unitless), f_t is the plant temperature constraint (unitless), f_m is the plant moisture constraint (unitless), f_{sm} is the soil moisture constraint (unitless), α is the PT coefficient (1.26), Δ is the slope of the saturated vapor pressure curve (kP$_a$°C^{-1}), γ is the psychrometric constant (0.066 kP$_a$°C^{-1}), G is the soil heat flux (W·m^{-2}), and R_{nc} is the net radiation for the canopy (W·m^{-2}) and is given by $R_{nc} = R_n - R_{ns}$, where R_n is the net radiation (W·m^{-2}) and R_{ns} is the net radiation for surface soil. R_{ns} can be calculated as [*Fisher et al.*, 2008; *Beer*, 1852; *Denmead and Millar*, 1976]

$$R_{ns} = R_n \exp(-k_{R_n} LAI) \tag{4}$$

where k_{Rn} is the extinction coefficient [*Impens and Lemeur*, 1969] and LAI is the leaf area index (m^2·m^{-2}), expressed as [*Fisher et al.*, 2008; *Ross*, 1976]

$$LAI = \frac{[\ln(1 - f_{IPAR})]}{k_{PAR}} \tag{5}$$

with $k_{PAR} = 0.5$ and f_{IPAR} is the fraction of photosynthesis active radiation (PAR) intercepted by canopy. The bio-physiological constraint functions are calculated as

$$f_{wet} = RH^4 \tag{6}$$

$$f_g = \frac{f_{APAR}}{f_{IPAR}} \tag{7}$$

$$f_t = \exp\left\{\left[-\left(\frac{T_a - T_{opt}}{T_{opt}}\right)^2\right]\right\} \tag{8}$$

$$f_m = \frac{f_{APAR}}{f_{APAR_{max}}} \tag{9}$$

$$f_{sm} = RH^{VPD/\beta} \tag{10}$$

where RH is relative humidity (%), T_a is the air temperature (°C), T_{opt} is the optimum plant growth temperature (°C), VPD is vapor pressure deficit (kPa), β is the sensitivity for f_{sm} to VPD (kPa), and f_{APAR} is the fraction of PAR absorbed by canopy. f_{IPAR} and f_{APAR} are defined as [*Fisher et al.*, 2008; *Gao and Li*, 2000; *Huete et al.*, 2002]

$$f_{APAR} = m_1 EVI + b_1 \tag{11}$$

$$f_{IPAR} = m_2 NDVI + b_2 \tag{12}$$

where EVI is the enhanced vegetation index; NDVI is the normalized difference vegetation index; and m_1, b_1, m_2, and b_2 are parameters. There are eight specific parameters in the PT-JPL model that need to be estimated (Table 2).

3.2. Global Sensitivity Analysis

The Sobol' method [*Sobol*, 1990, 2001] is a popular global sensitivity analysis based on variance decomposition and the model is represented in the following functional form

$$y = f\left(X, \vec{\theta}\right) \tag{13}$$

where y is the model output (or the result of objective function), X is the input variable, and $\vec{\theta}$ is the parameter vector. The total variance of function $D(y)$ can be decomposed into summands of increasing dimensionality, which can be expressed as

$$D(y) = \sum_{i=1}^{k} D_i + \sum_{i=1}^{k-1}\sum_{j=i+1}^{k} D_{ij} + \cdots + D_{1,\ldots,k} \tag{14}$$

where D_i is the partial variance with the first-order index of θ_i on the model output y, D_{ij} is the partial variance with the second-order index of the ith and jth parameter interactions, k is the total number of parameters. In this method, the sensitivity effect is characterized by the ratio of the partial variances to the total variance [*Zhang et al.*, 2013]:

$$\text{First-order index } S_i = \frac{D_i}{D} \tag{15}$$

$$\text{Second-order index } S_{ij} = \frac{D_{ij}}{D} \tag{16}$$

$$\text{Total-order index } S_{Ti} = S_i + \sum_{j \neq i} S_{ij} + \cdots = 1 - \frac{D_{\sim i}}{D} \tag{17}$$

where S_i is a measure ratio from the main effect of the individual parameter θ_i to the total model variance D, S_{ij} defines the sensitivity that results from the interactions between θ_i and θ_j, and S_{Ti} represents the main effect of θ_i and its interactions with the other parameters and can be calculated by the variance $D_{\sim i}$, which is the variation of all parameters except θ_i [*Homma and Saltelli*, 1996; *Nossent et al.*, 2011].

In our study, we used Latin hypercube sampling [*McKay*, 1988], a multidimensional, stratified sampling method [*Osidele and Beck*, 2001; *Sieber and Uhlenbrook*, 2005], to sample the available parameter space. A detailed description of the implemented computational process can be found in *Sobol* [1990, 2001], *Hall et al.* [2005], *Nossent et al.* [2011], and *Zhang et al.* [2013]. We also used the thresholds to differentiate highly sensitive parameters that contributed at least 10% of the overall model output variance and sensitive parameters that contributed at least 1% of the overall model output variance. When the contributions to the overall model output variance were less than 1%, we assumed that the parameters were nonsensitive [*Tang et al.*, 2007].

An important condition for running the PT-JPL model is the feasible range of the variable f_g. The energy absorbed by the canopy should not be greater than the intercept of energy (i.e., $f_g \leq 1$); hence, restrictions must be placed on the prior range of m_1 based on the related parameters: b_1, m_2, and b_2, which are the basic parameters of f_g. Additionally, we used a sample size of 10,000 to calculate the first-order and total-order sensitivity index of the eight parameters (Table 2) of the PT-JPL model.

3.3. Parameter Optimization With Differential Evolution Markov Chain

According to the Bayes theorem, the posterior probability density function (PDF) of model parameters is proportional to their prior PDF and the likelihood function and can be calculated as

$$p(\theta|O) \propto p(O|\theta)p(\theta) \tag{18}$$

where θ are the parameter sets; O are the observed data sets; $p(\theta|O)$ is the posterior probability distribution; $p(\theta)$ is the prior probability distribution of parameter θ, which is chosen as uniform distributions with specified prior ranges (Table 2); and $p(O|\theta)$ is the likelihood function, which reflects the influence of the observation data sets on parameter identification. The likelihood function can be expressed as [*Zhu et al.*, 2014]

$$p(O(t)|\theta) = \prod_{t=1}^{T} \frac{1}{\sqrt{2\pi\sigma^2}} \exp\left(-\frac{[O(t) - S(t)]^2}{2\sigma^2}\right) \tag{19}$$

where T is the total length of observation; $O(t)$ and $S(t)$ are observed and simulated values at time t ($t = 1, 2, \ldots, T$), respectively; and σ is the standard deviation of the model error that is assumed to be unchanged during the observation time [*Braswell et al.*, 2005], and σ can be expressed as

$$\sigma = \sqrt{\frac{1}{T}\sum_{t=1}^{T}[O(t) - S(t)]^2} \tag{20}$$

The posterior distribution was sampled by using the DE-MC method, which was proposed by *Ter Braak* [2006] for global optimization in real parameter spaces. In the DE-MC method, N chains are run in parallel and the proposals are generated on the basis of two randomly selected chains, the difference of which is multiplied by a scaling factor, and added to the current chain:

$$\theta_p = \theta_i + \gamma(\theta_{R1} - \theta_{R2}) + e \tag{21}$$

where θ_p is the proposed parameter set; θ_{R1} and θ_{R2} represent the randomly selected chains without replacement from the population θ_{-i} (the population without θ_i); e is drawn from a symmetrical distribution with a small variance compared to that of the target, but with unbounded support, e.g., $e \sim N(0,b)^d$ with b small and d being the parameter dimension; and γ is the scaling factor which can be set to be $2.38/\sqrt{2d}$ [*Roberts and Rosenthal*, 2001]. The Metropolis ratio is then used to decide whether to accept or reject the proposals [*Moreno et al.*, 2016].

3.4. Evaluation and Objective Function

Both the sensitivity analysis and optimization for the model need to consider goodness-of-fit metrics. We used the statistical metric root-mean-square error (RMSE) to evaluate the model output. The indicator can be calculated as

$$\text{RMSE} = \sqrt{\frac{1}{T} \sum_{t=1}^{T} [O(t) - S(t)]^2} \tag{22}$$

We also used the Nash-Sutcliffe efficiency (NSE) coefficient [*Nash and Sutcliffe*, 1970; *Legates and McCabe*, 1999] to evaluate the performance of the PT-JPL model:

$$\text{NSE} = 1 - \frac{\sum_{t=1}^{T} [O(t) - S(t)]^2}{\sum_{t=1}^{T} [O(t) - \overline{O}]^2} \tag{23}$$

where $\overline{O}$ is the mean of observed values. NSE values range between $-\infty$ to 1. Generally, as the value nears 1, a better simulation is indicated [*Moriasi et al.*, 2007; *Ershadi et al.*, 2014].

Additionally, to evaluate the final performance of the model, we used a Taylor diagram [*Taylor*, 2001] since this method is especially useful in testing multiple aspects of complex models [*International Panel on Climate Change*, 2001]. Generally, the Taylor diagram characterizes a single point to indicate three different statistical relationships between the "test" field (simulation) and the "truth" field (observation) (correlation, ratio of the standard deviations, and root-mean-square difference of the patterns) [*Zhu et al.*, 2016]. The statistics of each point can be scored using

$$S = \frac{2(1+R)}{[(\sigma_m/\sigma_o) + 1/(\sigma_m/\sigma_o)]^2} \tag{24}$$

where S is the model skill metric bound by zero and unity (unity indicates agreement with observations), σ_m is the standard deviation of the simulation, and σ_o is the standard deviation of the observation.

4. Results

4.1. Parameter Sensitivity Analysis

The sensitivity index (SI) of model parameters across different sites based on the RMSE metric is illustrated in Figure 2. Based on threshold in *Tang et al.* [2007], three parameters (m_1, T_{opt}, and β) across all the biomes were most sensitive, while other parameters were nonsensitive to the model output. Figure 2a (S_i) shows that the parameter m_1 has the most significant single influence on the model ET simulation across different biomes (SI value varies from 2% at site US-FR3 to 98% at site CN-Cha; mean value was 48%). Also, the parameters T_{opt} and β had high first-order SI, although their SI values were 2–3 times smaller than that of m_1. Moreover, T_{opt} has a higher first-order SI than β in the forest biomes (mixed forest, evergreen broadleaf forest, and deciduous broadleaf forest). The contribution of the remaining parameters at each site is almost negligible.
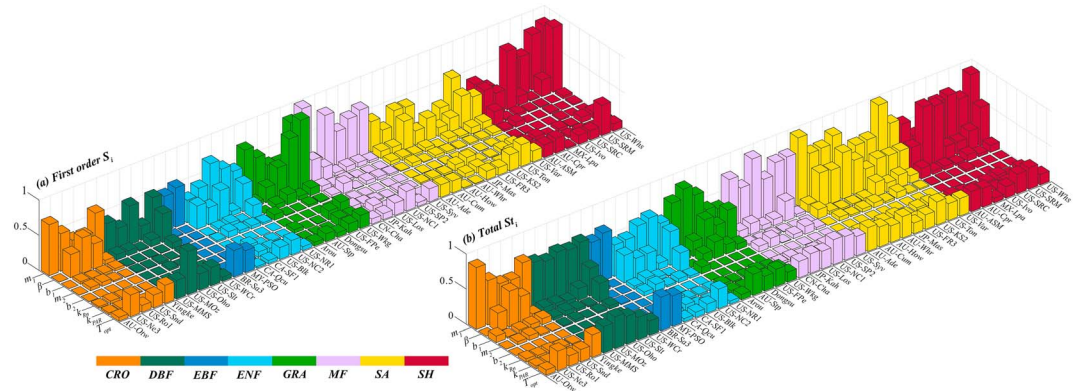
Figure 2. Results of sensitivity analysis using the Sobol' method. (a) and (b) represent the first and total order sensitivity index, respectively. Different colors indicate different biomes.

Similarly, these three parameters are also highly sensitive with a total order index greater than 10% across most sites (Figure 2b). The parameter m_1 has the most significant influence, accounting for a maximum of 99% (at US-Ton), a minimum of 14% (at MX-Lpa), and a mean of 65% of the total variance. Combined, these three parameters (m_1, T_{opt}, and β) are the most influential on the model output. It should be noted that the first-order SI of the parameters contributed the highest proportion of the total order SI at most sites. Furthermore, the forest biomes, especially the DBF, EBF, and MF, have larger total order SI of m_1 than the other parameters. It seems that m_1, related to the canopy constraint factor (f_g), has more interactions with other parameters in the forest biomes. Additionally, it is interesting to note the proportion of the influence of m_1 interactions on the model output to the total order SI increases gradually in comparison with the parameter T_{opt} and β. Overall, the output of the PT-JPL model is highly sensitive to the parameters m_1, T_{opt}, and β across the different biomes.

4.2. Parameter Optimization

The posterior parameter distributions (medians and 95% probability intervals) of the three sensitive parameters are shown in Figure 3. The results indicate that the Bayesian optimization with DE-MC method successfully reduced the assumed prior uncertainties of the sensitive parameters in most sites. T_{opt} and β showed relatively large uncertainty and variability (widely spread on the prior ranges) in some sites.
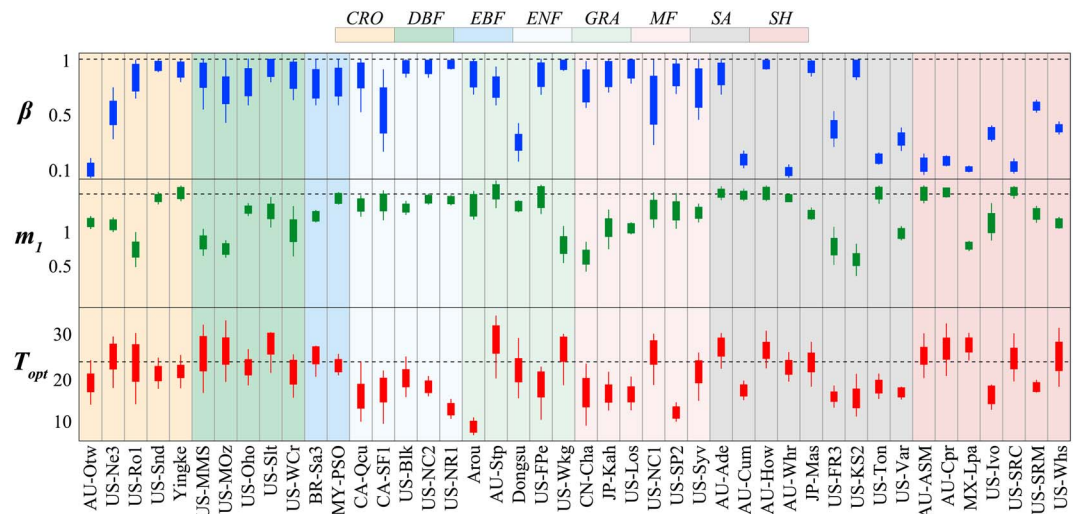

Figure 3. Posterior distribution of the parameters at each site. The vertical bars indicate the 95% probability intervals; the dot line represents the original parameter value.
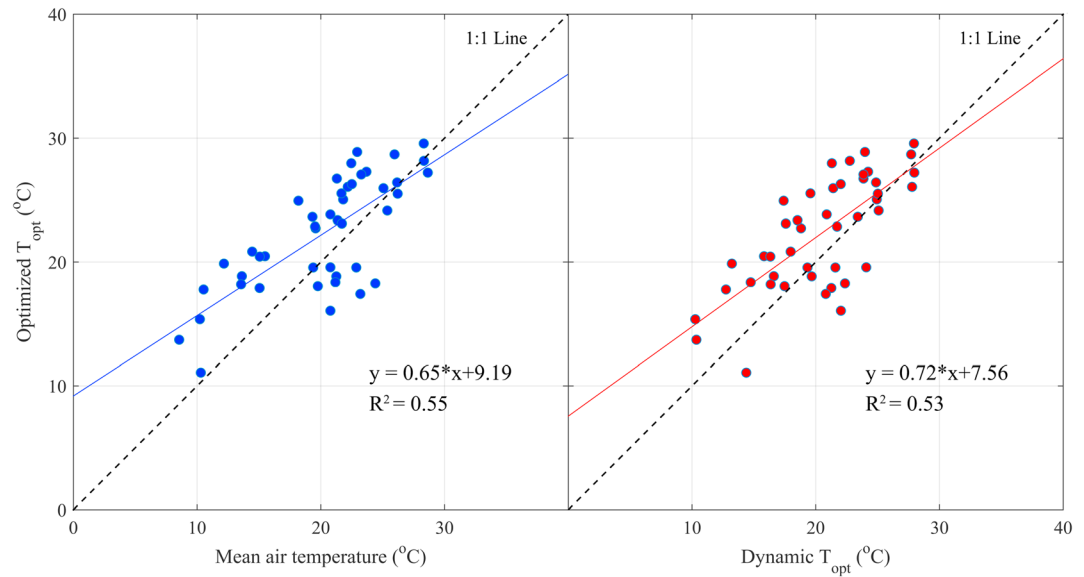
Figure 4. Relationships between optimized T_{opt} and mean air temperature and dynamic T_{opt} for different biomes during the study period.

The posterior median values of β in the AU-Otw, AU-Cum, AU-Whr, US-Ton, AU-ASM, AU-Cpr, MX-Lpa, and US-SRC sites were very small (<0.2). At US-Ne3, Dongsu, US-FR3, US-Var, US-Ivo, and US-SRM, as well as the US-Whs site, the optimized values of β remained within a relatively low range (0.3–0.5). The optimized values of β at most sites (e.g., US-Ro1, US-Snd, US-MMS, Arou, and AU-How) range from 0.6 to 1. Thus, it seems that the responses of surface constraint (β) to soil water content should be enhanced at different sites, especially in arid environments.

The optimized median value of m_1 ranged from 0.63 (US-KS2) to 1.39 (AU-Stp) with a mean value of 1.1 across different biomes (Figure 3). Generally, the posterior median values of m_1 are relatively low (around 0.8–1.3) across mostly forest biomes (DBF and MF). However, the posterior median values in the some savannas and grasslands sites are slightly higher, ranging from 1.1 to 1.4. Thus, we concluded that the parameter m_1 was properly optimized for each site because the 95% posterior distribution of m_1 was narrow. Notably, the optimized mean median value of different biomes is slightly lower than the original value (1.36) proposed by *Fisher et al.* [2008].

T_{opt} exhibited a very wide variation across different biomes with a minimum value of 11°C (Arou) and a maximum value of 29°C (AU-Stp) (Figure 3). The parameter T_{opt} represents the optimum plant growth temperature under specific environments. Thus, we investigated the relationship between optimized T_{opt} and the mean air temperature (T_a) during growing season and found the correlation between these variables is relatively high ($R^2 = 0.55$; Figure 4). Some authors have proposed that T_{opt} should be dynamically calculated based on the maximum temperature at the time of peak canopy activity (hereafter referred to as the dynamic method [*Potter et al.*, 1993; *Fisher et al.*, 2008]). The optimized values of T_{opt} obtained by our procedure also exhibited good agreement with those calculated by using the dynamic method (Figure 4), suggesting that our optimized values are reasonable.

4.3. Model Performance: PT-JPL Model With Optimized Parameters

Figure 5 and Table 3 compare the model performance by using the optimized and the original parameters against the directly observed latent heat fluxes. In addition, the model performances evaluating against the corrected latent heat fluxes were presented in the supporting information. Generally, the models had similar R ranges (mostly ranging between 0.6 and 0.9); however, the model using optimized parameters performed better with σ_{norm} (normalized standard deviations) nearer to 1 (Figure 5), lower bias and RMSE, and greater NSE (Table 3). The model using original parameters overestimated evapotranspiration in most cases (particularly in shrublands) (i.e., NSE < 0, σ_{norm} > 1.5).
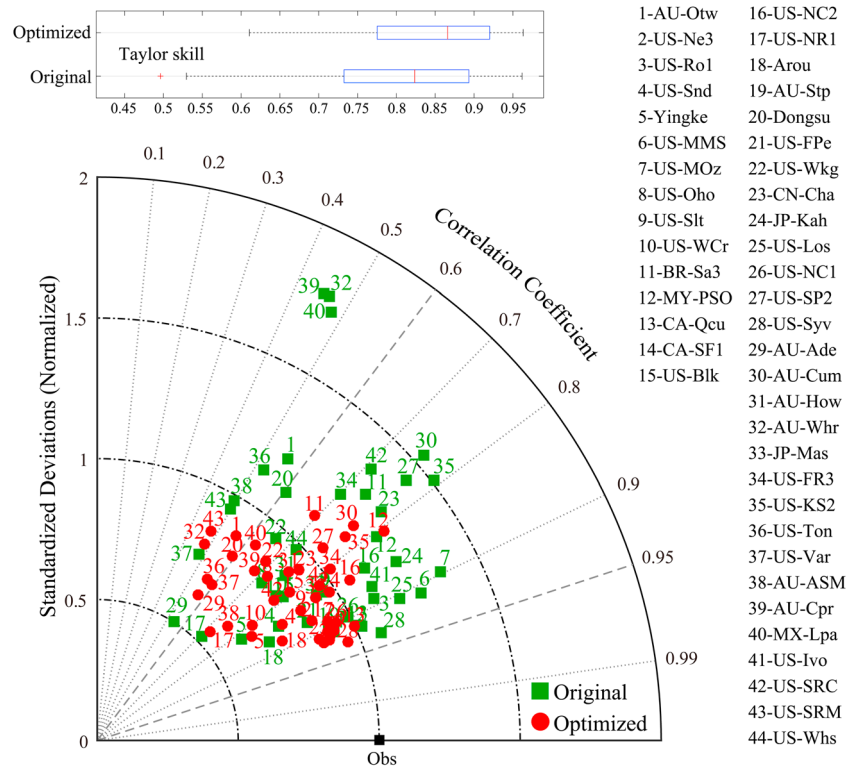
Figure 5. Taylor diagram displaying a statistical comparison of model performance using original and optimized parameters across different sites.

As expected, the performance of both models showed a high degree of site-specific variation across different biomes. For example, both performed well at some grasslands (Arou, AU-Stp, and US-FPe) and croplands (US-Ne3, US-Ro1, and US-Snd) sites. However, at most sites (especially Dongsu, MX-Lpa, and AU-Cpr), the original model overestimated evapotranspiration (Figure 5 and Table 3). The optimized model across the different sites showed results of σ_{norm} clustered around 1, which is more in line with observed measurements than the results for the original model.

Generally, the original model performance was satisfactory across some croplands and grasslands (except for AU-Otw and Dongsu), with R^2 values ranging from 0.31 to 0.84 and NSE values greater than 0.31 (Table 3). At 14 of the 44 sites, the original model generated negative NSE, because it overestimated ET significantly, with bias < 0 (Table 3). In contrast, the NSE values generated by the PT-JPL model with optimized parameters are greater than zero at all sites and are near 1 at some sites (US-Syv, US-Ne3, US-Ro1, and AU-Stp) (Table 3). It is worth noting that the slope and R^2 of the regression equation for the modeled and observed ET varied depending on the model used (original versus optimized parameters). Therefore, the model with optimized parameters can greatly improve the reliability of PT-JPL in these different sites.

We selected four typical sites (US-Ne3, US-MMS, AU-Cum, and MX-Lpa) to show the difference temporal variation between observed and estimated ET using the original and optimized models (Figure 6). In these cases, the optimized model effectively eliminated ET overestimation and exhibited an obvious improvement compared to original model (c- AU-Cum and d-MX-Lpa). The original model had satisfactory performance in the croplands with relatively homogenized surface and adequate soil moisture (US-Ne3; Figure 6a). Also, the results in Table S2 in the supporting information indicated that the optimized model performed better at most sites than the original model even when evaluating against the corrected latent heat fluxes. Thus, the model parameter uncertainty seems to be the main source of the disagreements between the simulated and observed (corrected) latent heat fluxes.

Table 3. Summary of Statistical Performance of the Original and Optimized Model Over Different PFTs During the Study Period[a]

Site		Original						Optimized					
Name	ID	R^2	Slope	d	Bias	RMSE	NSE	R^2	Slope	d	Bias	RMSE	NSE
AU-Otw	S1	0.31	**0.7**	37.4	−21.8	38.9	−0.67	**0.32**	0.49	**22.1**	**3.8**	**26.9**	**0.2**
US-Ne3	S2	**0.84**	**0.93**	11.4	−8.5	21.5	0.8	**0.84**	0.81	**9.7**	**−1.2**	**19.4**	**0.84**
US-Ro1	S3	0.79	**0.95**	7.3	−5	22.7	0.75	**0.84**	0.82	**6.8**	1.7	**18**	**0.84**
US-Snd	S4	0.67	0.65	14.6	**3.8**	20	0.66	**0.7**	**0.67**	**13.6**	4	**19.1**	**0.69**
Yinke	S5	0.57	0.48	36.9	14.9	32.8	0.44	**0.66**	**0.53**	**33.7**	13	**29.6**	**0.54**
US-MMS	S6	**0.83**	**1.14**	**12.3**	−18.4	27	0.45	0.82	0.82	12.6	−4.8	**16.2**	**0.8**
US-MOz	S7	0.43	0.47	17.5	2.7	26.9	0.42	**0.79**	**0.82**	**9.2**	**−2.3**	**16.5**	**0.78**
US-Oho	S8	0.54	0.44	4.2	**25.2**	46.6	0.32	**0.6**	**0.48**	**1.8**	25.2	**44.6**	**0.38**
US-Slt	S9	0.62	0.67	14.5	−1	24.3	0.61	**0.71**	**0.72**	**10.2**	1.2	**21.2**	**0.71**
US-WCr	S10	0.41	0.39	24.1	3.9	35.1	0.41	**0.64**	**0.55**	**20.2**	0.6	**27.7**	**0.63**
BR-Sa3	S11	**0.55**	**1**	**13.5**	−13.6	21.1	−0.39	0.49	0.81	16.6	1.5	**15.2**	**0.28**
MY-PSO	S12	**0.69**	**1.02**	−8.8	6.9	16.7	0.42	0.68	1.04	**−8.6**	4.7	**16.2**	**0.46**
CA-Qcu	S13	0.78	0.66	**−0.9**	8.5	13.9	0.62	**0.83**	**0.91**	−2.9	4.8	**10.5**	**0.78**
CA-SF1	S14	0.58	0.44	7.5	13.2	25.3	0.37	**0.79**	**0.84**	**2.5**	**3.6**	**15**	**0.78**
US-Blk	S15	0.48	0.52	6.2	**14**	28.3	0.31	**0.57**	**0.55**	**4.9**	14	**26.5**	**0.4**
US-NC2	S16	**0.71**	**0.95**	−10.2	**14**	29.3	0.51	**0.71**	0.9	**−7.9**	16.2	**29.1**	**0.52**
US-NR1	S17	0.4	0.39	11.4	25.8	40.3	−0.01	**0.5**	**0.46**	**9.5**	**23.5**	**36.9**	**0.15**
Arou	S18	**0.81**	**0.91**	−5.3	13.3	19	0.6	**0.81**	0.9	**−3.5**	**12**	**18**	**0.64**
AU-Stp	S19	0.76	**0.76**	7.5	−1.9	15.4	0.76	**0.77**	0.74	**5.3**	**0.9**	**15.2**	**0.77**
Dongsu	S20	0.27	**0.63**	20.8	−10.9	19.7	−0.74	**0.35**	0.42	**13.4**	**2.4**	**12.4**	**0.31**
US-FPe	S21	0.7	**0.83**	3.4	**1.6**	15.3	0.67	**0.73**	**0.83**	**3.2**	2	**14.5**	**0.71**
US-Wkg	S22	0.44	**0.63**	11	−4.2	17.5	0.31	**0.47**	0.6	**6.4**	**0.9**	**15.9**	**0.43**
CN-Cha	S23	**0.6**	**1.03**	7.1	−7.7	25.1	0.23	0.58	0.72	**6.4**	**1**	**19.1**	**0.55**
JP-Kah	S24	**0.73**	**0.95**	**8.5**	−5.7	20.8	0.63	0.71	0.82	8.6	**0.6**	**19.2**	**0.69**
US-Los	S25	**0.83**	**1.11**	**6.5**	−9.6	17	0.6	**0.83**	0.79	7.2	**−1.4**	**11.4**	**0.82**
US-NC1	S26	0.79	**0.97**	−2.9	**4.6**	**20.4**	**0.74**	0.79	0.89	**−2.2**	9.2	21.1	**0.74**
US-SP2	S27	0.43	**1.23**	23.9	−34.9	43.9	−4.52	0.3	0.52	24.4	**−1.4**	**17.4**	**0.14**
US-Syv	S28	**0.87**	**1.02**	3.6	−4.3	14.6	0.82	**0.87**	0.89	**3.4**	**0.6**	**12.7**	**0.87**
AU-Ade	S29	0.28	0.26	52.9	**−4.8**	30	0.26	**0.32**	**0.3**	**50.4**	−4.9	**29.1**	**0.3**
AU-Cum	S30	**0.43**	1.27	**4.7**	−19	39	−1.89	0.41	**0.76**	6.8	5.9	**22.5**	**0.04**
AU-How	S31	**0.54**	**0.77**	**12.9**	9.9	27.1	0.36	**0.54**	**0.77**	13.4	9.1	**26.9**	**0.37**
AU-Whr	S32	0.23	**0.9**	13	−9.5	23.4	−2.22	**0.31**	0.55	**11.8**	3.8	**12.8**	**0.03**
JP-Mas	S33	**0.69**	**0.82**	**3.3**	**11.2**	**27.3**	**0.6**	**0.69**	0.78	4.2	13.2	28.1	**0.6**
US-FR3	S34	0.49	**0.9**	15.7	−11.5	24.9	−0.08	**0.55**	0.78	**3.6**	**5.6**	**18.4**	**0.41**
US-KS2	S35	**0.59**	1.15	14.6	−26.3	40.9	−0.6	0.57	0.81	18.4	**−3.5**	**23.9**	**0.45**
US-Ton	S36	0.25	**0.57**	22.3	−10.3	27.7	−0.39	**0.32**	0.33	**15.6**	3.1	**19.7**	**0.3**
US-Var	S37	0.35	**0.48**	16.7	−4.4	22.5	0.28	**0.37**	0.41	**13.6**	0.3	**21.1**	**0.37**
AU-ASM	S38	0.23	**0.48**	16.6	−10.3	18.6	−0.5	**0.56**	0.31	**5.2**	3.2	**11.7**	**0.41**
AU-Cpr	S39	0.18	**0.77**	20.9	−16.7	24.2	−4.28	**0.46**	0.56	**7.3**	**1**	**8**	**0.43**
MX-Lpa	S40	0.18	0.73	46.5	−42.2	47	−11.42	**0.35**	0.51	**10.7**	**−2.9**	**11.8**	**0.22**
US-Ivo	S41	0.33	0.6	7.7	4.3	19.2	0.07	**0.65**	**0.9**	**2.9**	0.1	**13.2**	**0.56**
US-SRC	S42	0.51	**0.97**	9.6	−9.2	16	−0.38	**0.62**	0.57	**3.1**	2.8	**8.9**	**0.57**
US-SRM	S43	**0.26**	**0.49**	13.6	−4	15.7	−0.01	0.21	0.35	**8.8**	3.3	**14.9**	**0.08**
US-Whs	S44	**0.54**	**0.74**	11.6	−7.3	16.7	0.33	0.41	0.45	**5.3**	3.8	**16.2**	**0.38**

[a]The bold font represents the best performance and d represents the intercept.

5. Discussion

Evaluating model uncertainties is a persistent challenge in hydrological modeling [*Beven et al.*, 2008]. Understanding the influence of model parameters and biome types on model response is significant elements in the development of robust regional and global ET products [*Bastola et al.*, 2011; *Brigode et al.*, 2013; *McCabe et al.*, 2016]. However, the uncertainties and sensitivity of model parameters may change with different biomes and climate conditions. Many ecophysiological parameters of the PT-JPL model are needed to identify the key parameters and optimize them to obtain reliable estimation of ET. Previous studies [*Fisher et al.*, 2008; *Garcia et al.*, 2013] focused on the model's sensitivity to forcing data. Nevertheless, specific biomes and climate zones present different uncertainties and variations in the sensitivity of parameters in
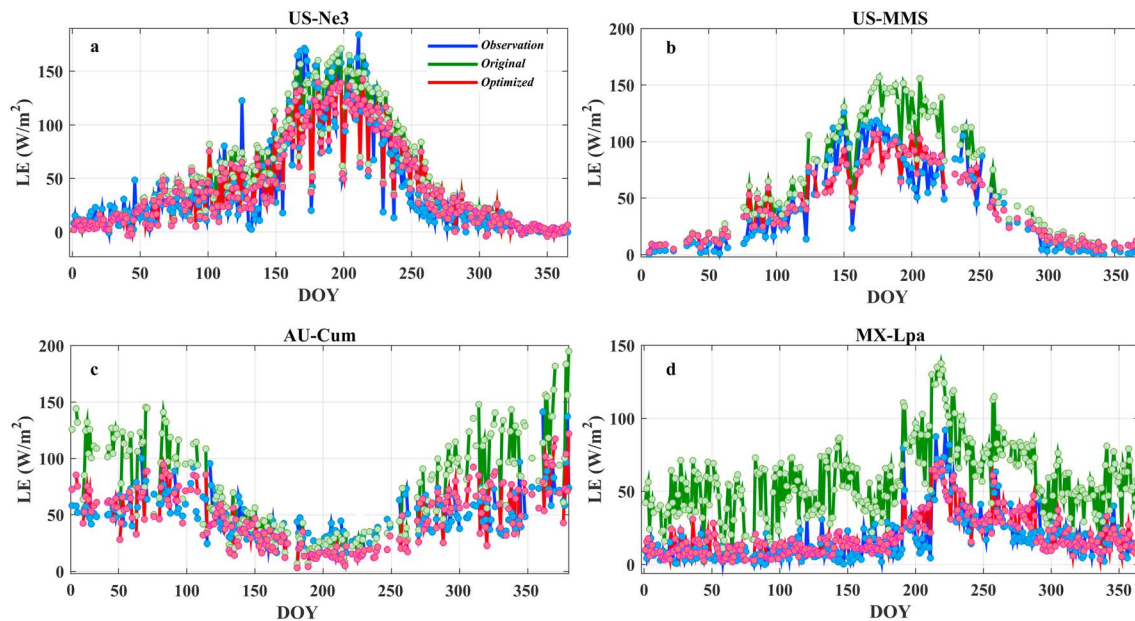
Figure 6. Comparison LE of observed, original model and optimized model in four different sites during the study period. (a) US-Ne3 site (croplands), (b) US-MMS site (deciduous broadleaf forest), (c) AU-Cum (savannas), and (d) MX-Lpa (shrublands).

the PT-JPL model due to the main driving forces (i.e., net radiation, RH, and vegetation index) [*Yao et al.*, 2013, 2014; *Fisher et al.*, 2008; *Feng et al.*, 2015]. Thus, it may be more meaningful to investigate the sensitivity of parameters across different biomes and climate conditions. Our results indicated that three of the eight parameters β, m_1, and T_{opt} are sensitive to the simulated ET of the PT-JPL model across different biomes. These three parameters are related to the process of energy constraint, soil evaporation, and plant growing temperature.

Overall, we attempted to quantify the uncertainty of the PT-JPL model at multiple sites across diverse biomes for the purpose of optimizing the sensitive parameters to the specific biomes. At the sites with low vegetative cover (low NDVI and EVI) and low precipitation (e.g., Dongsu and MX-Lpa), β was more sensitive than other parameters in the PT-JPL model. This is because under these conditions, the soil receives more energy than the canopy during the process of energy (net radiation) partition. Hence, the total ET is dominated by soil evaporation (ET_s) and restricted by the constraint variable f_{sm} (based on β). Therefore, the variation of β has the most significant impact on the ET_s simulation in arid areas with low vegetation. Our results are consistent with previous studies where f_{sm} played a primary role in model uncertainty in drylands [*Garcia et al.*, 2013]. Bio-constraints (i.e., f_g, f_m, and f_T) dominate the canopy transpiration in relatively humid regions with high NDVI. These bio-constraints are directly reflected in the parameters m_1, b_1, m_2, b_2, and T_{opt} (Table 2). We found that m_1 had a large influence on the model performance at most sites with good vegetative conditions, such as Arou, US-Ro1, and the forest sites. Arou is alpine grasslands on Qinghai-Tibetan Plateau with adequate moisture, and the ET is strongly limited by energy [*Zhu et al.*, 2016]. This may be the reason m_1 contributed a peak SI to the model performance at most sites. Thus, it is crucial to use a proper value of m_1 to estimate ET with the PT-JPL model. Furthermore, T_{opt} is a basic parameter to the bio-constraint variable f_T and ranked second in the first-order SI in the most forest biomes. However, we noted that the total SI of f_T was surpassed by β in the ENF sites. This may be a result of the increasing interaction impact of β with specific site conditions (e.g., CA-SF1 site with relatively low EVI and precipitation).

Although the performance of the PT-JPL model was evaluated as good compared to other remote sensing ET models in recent studies [*McCabe et al.*, 2016; *Ershadi et al.*, 2014; *Zhu et al.*, 2016], data are insufficient to demonstrate that it provides consistently good simulations over a wide range of biomes and different temporal scales [*Vinukollu et al.*, 2011; *Mallick et al.*, 2013; *Garcia et al.*, 2013; *Michel et al.*, 2016]. Generally, poorer performance has been shown by *McCabe et al.* [2016] and *Garcia et al.* [2013] for arid regions. Our evaluation

also indicates similar poor performance at Dongsu (arid grasslands, overestimated), AU-Cpr (shrublands, overestimated), and US-NR1 (ENF, underestimated) (Figures 5 and 6 and Table 3). The original PT-JPL model seems most suitable for regions with relatively homogenized surfaces and sufficient moisture, such as Arou and US-Ro1.

The large variability in the SI of some of the model parameters (Figure 2) indicates that the use of constant values to model under different biomes for regional and global applications is inappropriate. Thus, it is critical to optimize the key parameters of the PT-JPL model for different environments. We constructed a Bayesian inference framework to optimize the key parameters using the flux data sets simultaneously. But, an important issue in optimization is equifinality, where the same result might be caused by different parameter combinations [*Franks et al.*, 1997; *Zhu et al.*, 2014]. *Engeland et al.* [2006], *Fenicia et al.* [2007], *Moussa and Chahinian* [2009], and *Hrachowitz et al.* [2013] have indicated that multiple objective calibration and data sets could provide effective optimization against equifinality. To minimize the problem of equifinality, we ran the model for different sites and performed the DE-MC method searches for the parameter space using different chains.

As shown in Figure 3, the parameter m_1 (related to canopy resistance) seemed to be optimized with relatively narrow uncertainties (95% posterior distribution performed stably between 0.6 to 1.4) at different sites. The original model slightly overestimated m_1 at some specific sites, especially in the forest biomes with relative higher canopy (DBF, EBF, and MF). Similar performance has been reported by *Mallick et al.* [2013], with the mean bias revealing a consistent overestimation at a majority of sites. Our model with optimized parameters addressed this problem by reducing the value of the most sensitive parameter (m_1) from an original constant value of 1.36 to an optimized value of the posterior distribution in 95% high-probability intervals (Table 2 and Figures 3 and 4). The results indicate that the strength of energy constraints (i.e., f_g, f_m, and f_T) on the canopy in the original PT-JPL model may not be sufficient, especially in the DBF and MF.

To avoid the calibrations being dependent on each site, *Garcia et al.* [2013] and *Yao et al.* [2013, 2014] set the optimum temperature (T_{opt}) at 25°C, rather than being dynamically calculated as in the original PT-JPL model [*Fisher et al.*, 2008; *Ershadi et al.*, 2014]. Although this value has been used in many modeling studies across different biomes [*Yuan et al.*, 2010], the optimum vegetation temperature T_{opt} should be more reflective of the specific region [*Cui*, 2013]. The original calculation of T_{opt} was prone to be unreliable in some specific biomes and climate conditions, such as Mediterranean semiarid environments [*Garcia et al.*, 2013]. For our study, we obtained optimized T_{opt} sets (Figure 3) for each site. Figure 4 illustrates that these had good correlation to the measured mean air temperature (growing season), with the optimized model showing a slight improvement over the original model (Figures 5 and 6). This provides a convenient way to simultaneously run the model at different biomes when the air temperature data are available.

The parameter β is a unique constant parameter that influences the estimation of soil evaporation. As has long been discussed [*Garcia et al.*, 2013], the value of β should be fine-tuned in different regions to obtain reliable results, and *Fisher et al.* [2008] developed the original PT-JPL model and applied $\beta = 1$ kPa, but *Mu et al.* [2007] used $\beta = 0.1$ kPa for a global application. ET estimates using the original PT-JPL model ($\beta = 1$ kPa) did not provide meaningful results in specific regions, such as in Mediterranean grasslands [*Garcia et al.*, 2013] and drylands (Dongsu, AU-ASM, AU-Cpr, MX-Lpa, etc.) (Figures 5 and 6 and Table 3). Table 3 and Figure 5 indicate the results when model was run with a median value of 95% high-probability intervals after optimization. β was reduced at most sites and diverged more regularly in some arid regions, suggesting that the control of the soil moisture stress derived from atmospheric conditions (i.e., relative humidity or VPD) should be strengthened. For example, at the AU-Cpr site (the South Australian shrublands with BSk climate and low vegetation cover), β was revised to a minimal value (0.1). This may indicate that the contribution from ET_s to total ET was strongly limited by the soil moisture as depicted by β and atmospheric conditions [*Mu et al.*, 2007; *Yao et al.*, 2013]. Even at the Dongsu site (Grasslands with annual precipitation under 300 mm) (Table 1), the optimized β value decreased from the original (Figure 3).

Fundamentally, the SA and optimization method in this study could identify and optimize the common key parameters of the PT-JPL model across different biomes. Furthermore, the main source of model error is attributable to the model structure once the parameters have been optimized using the DE-MC method [*Zhu et al.*, 2014], although the performance of the optimized model varied by region. Thus, the optimization of the PT-JPL model can lead to more robust ET flux estimation and reduce the uncertainty in regional ET estimation.

6. Conclusions

To generate a reliable long-term regional/global terrestrial ET product using the PT-JPL model, special attention should be paid on calibrating these parameters. As a result, our model with optimized parameters performed better than the original model at the selected study sites, especially in arid savannas and shrublands.

In the arid environment, the lower value of β provides a more intense constraint on soil evaporation that better depicts the limiting process of soil moisture. The parameter m_1, an important component of the model's interim variable f_g, plays a role to restrain the canopy energy to the actual ET. The optimized median value of m_1 was slightly lower than the value provided by the original model in a majority of biomes. This illustrates that the actual ET from the canopy in these biomes are under a stronger constraint than represented in the original model. Another canopy constraint parameter, T_{opt}, is also sensitive to the model across the different biomes. The optimized value at most sites was set around 25°C corresponding to the original model. But for a few sites, located in high altitudes or latitude with cold climate condition, the optimized value of T_{opt} was set in a lower range (10°C to 15°C). This result is nearer a realistic environmental temperature in the specific biomes and shows a more meaningful optimum temperature to the vegetation that grows in cold weather. The optimized values of T_{opt} obtained by our procedure also exhibited good agreement with those calculated using the dynamic method (Figure 4), suggesting that our optimized values are reasonable. Therefore, to obtain reliable global/regional ET products, the values of T_{opt} should be based on specific biomes and climate conditions rather than using a constant value (i.e., 25°C).

We suggest that the PT-JPL model be used with different parameter sets to obtain a more reliable output at the daily temporal scale, particularly in calculating the ET for the cold and arid biomes. In addition, all of the optimizations in this paper were focused on the parameter itself rather than the model structure.

References

AghaKouchak, A., A. Farahmand, F. S. Melton, J. Teixeira, M. C. Anderson, B. D. Wardlow, and C. R. Hain (2015), Remote sensing of drought: Progress, challenges and opportunities, *Rev. Geophys.*, 53, 452–480, doi:10.1002/2014RG000456.

Baldocchi, D., et al. (2001), FLUXNET: A new tool to study the temporal and spatial variability of ecosystem-scale carbon dioxide, water vapor, and energy flux densities, *Bull. Am. Meteorol. Soc.*, 82(11), 2415–2434.

Bastiaanssen, W. G. M., M. Menenti, R. A. Feddes, and A. A. M. Holtslag (1998), A remote sensing surface energy balance algorithm for land (SEBAL)—1. Formulation, *J. Hydrol.*, 212(1–4), 198–212.

Bastola, S., C. Murphy, and J. Sweeney (2011), The role of hydrological modelling uncertainties in climate change impact assessments of Irish river catchments, *Adv. Water Resour.*, 34(5), 562–576.

Baumgartner, A., and E. Reichel (1975), *The World Water Balance: Mean Annual Global, Continental and Maritime Precipitation, Evaporation and Run-off*, Elsevier Scientific Publishing Co., Amsterdam.

Beer, A. (1852), Bestimmung der Absorption des rothen Lichts in farbigen Flüssigkeiten, *Ann. Phys.*, 162, 77–88.

Bell, T. W., O. Menzer, E. Troyo-Diequez, and W. C. Oechel (2012), Carbon dioxide exchange over multiple temporal scales in an arid shrub ecosystem near La Paz, Baja California Sur, Mexico, *Global Change Biol.*, 18(8), 2570–2582.

Beringer, J., et al. (2016), An introduction to the Australian and New Zealand flux tower network—OzFlux, *Biogeosciences*, 13(21), 5895–5916.

Beven, K. J., P. J. Smith, and J. E. Freer (2008), So just why would a modeller choose to be incoherent?, *J. Hydrol.*, 354(1–4), 15–32.

Braswell, B. H., W. J. Sacks, E. Linder, and D. S. Schimel (2005), Estimating diurnal to annual ecosystem parameters by synthesis of a carbon flux model with eddy covariance net ecosystem exchange observations, *Global Change Biol.*, 11(2), 335–355.

Brigode, P., L. Oudin, and C. Perrin (2013), Hydrological model parameter instability: A source of additional uncertainty in estimating the hydrological impacts of climate change?, *J. Hydrol.*, 476, 410–425.

Bunting, D. P., S. A. Kurc, E. P. Glenn, P. L. Nagler, and R. L. Scott (2014), Insights for empirically modeling evapotranspiration influenced by riparian and upland vegetation in semiarid regions, *J. Arid Environ.*, 111, 42–52.

Chahine, M. T. (1992), The hydrologic cycle and its influence on climate, *Nature*, 359, 373–380.

Clark, J. S., and A. E. Gelfand (2006), A future for models and data in environmental science, *Trends Ecol. Evol.*, 21(7), 375–380.

Cleugh, H. A., R. Leuning, Q. Z. Mu, and S. W. Running (2007), Regional evaporation estimates from flux tower and MODIS satellite data, *Remote Sens. Environ.*, 106(3), 285–304.

Confalonieri, R., S. Bregaglio, and M. Acutis (2010), A proposal of an indicator for quantifying model robustness based on the relationship between variability of errors and of explored conditions, *Ecol. Model*, 221(6), 960–964.

Cui, Y. P. (2013), Preliminary estimation of the realistic optimum temperature for vegetation growth in China, *Environ. Manage.*, 52(1), 151–162.

Denmead, O. T., and B. D. Millar (1976), Field studies of the conductance of wheat leaves and transpiration, *Agron. J.*, 68(2), 307–311.

Dodds, P. E., W. S. Meyer, and A. Barton (2005), A review of methods to estimate irrigated reference crop evapotranspiration across Australia. CRC for Irrigation Futures Technical Report No. 04/05. CSIRO, Australia.

Engeland, K., I. Braud, L. Gottschalk, and E. Leblois (2006), Multi-objective regional modelling, *J. Hydrol.*, 327(3–4), 339–351.

Ershadi, A., M. F. McCabe, J. P. Evans, N. W. Chaney, and E. F. Wood (2014), Multi-site evaluation of terrestrial evaporation models using FLUXNET data, *Agric. For. Meteorol.*, 187, 46–61.

Feng, F., J. Q. Chen, X. L. Li, Y. J. Yao, S. L. Liang, M. Liu, N. N. Zhang, Y. Guo, J. Yu, and M. M. Sun (2015), Validity of five satellite-based latent heat flux algorithms for semi-arid ecosystems, *Remote Sens-Basel*, 7(12), 16,733–16,755.

Fenicia, F., H. H. G. Savenije, P. Matgen, and L. Pfister (2007), A comparison of alternative multiobjective calibration strategies for hydrological modeling, *Water Resour. Res.*, 43, W03434, doi:10.1029/2006WR005098.

Fisher, J. B., K. P. Tu, and D. D. Baldocchi (2008), Global estimates of the land-atmosphere water flux based on monthly AVHRR and ISLSCP-II data, validated at 16 FLUXNET sites, *Remote Sens. Environ.*, *112*(3), 901–919.

Fraedrich, D., and A. Goldberg (2000), A methodological framework for the validation of predictive simulations, *Eur. J. Oper. Res.*, *124*(1), 55–62.

Franks, S. W., K. J. Beven, P. F. Quinn, and I. R. Wright (1997), On the sensitivity of soil-vegetation-atmosphere transfer (SVAT) schemes: Equifinality and the problem of robust calibration, *Agric. For. Meteorol.*, *86*(1–2), 63–75.

Fu, G. T., Z. Kapelan, and P. Reed (2012), Reducing the complexity of multiobjective water distribution system optimization through global sensitivity analysis, *J. Water Res. Pl-Asce*, *138*(3), 196–207.

Fu, D., B. Chen, H. Zhang, J. Wang, T. A. Black, B. D. Amiro, G. Bohrer, P. Bolstad, R. Coulter, and A. F. Rahman (2014), Estimating landscape net ecosystem exchange at high spatial–temporal resolution based on Landsat data, an improved upscaling model framework, and eddy covariance flux measurements, *Remote Sens. Environ.*, *141*, 90–104.

Gao, B. C., and R. R. Li (2000), Quantitative improvement in the estimates of NDVI values from remotely sensed data by correcting thin cirrus scattering effects, *Remote Sens. Environ.*, *74*(3), 494–502.

Garcia, M., I. Sandholt, P. Ceccato, M. Ridler, E. Mougin, L. Kergoat, L. Morillas, F. Timouk, R. Fensholt, and F. Domingo (2013), Actual evapo-transpiration in drylands derived from in-situ and satellite data: Assessing biophysical constraints, *Remote Sens. Environ.*, *131*, 103–118.

Haario, H., M. Laine, A. Mira, and E. Saksman (2006), DRAM: Efficient adaptive MCMC, *Stat. Comput.*, *16*(4), 339–354.

Hall, B. D., H. Manolopoulos, J. P. Hurley, J. J. Schauer, V. L. S. Louis, D. Kenski, J. Graydon, C. L. Babiarz, L. B. Cleckner, and G. J. Keeler (2005), Methyl and total mercury in precipitation in the Great Lakes region, *Atmos. Environ.*, *39*(39), 7557–7569.

Heinsch, F. A., J. L. Heilman, K. J. McInnes, D. R. Cobos, D. A. Zuberer, and D. L. Roelke (2004), Carbon dioxide exchange in a high marsh on the Texas Gulf Coast: Effects of freshwater availability, *Agric. For. Meteorol.*, *125*(1–2), 159–172.

Hollinger, D. Y., et al. (2010), Albedo estimates for land surface models and support for a new paradigm based on foliage nitrogen con-centration, *Global Change Biol.*, *16*(2), 696–710.

Homma, T., and A. Saltelli (1996), Importance measures in global sensitivity analysis of nonlinear models, *Reliab. Eng. Syst. Safe*, *52*(1), 1–1.

Hrachowitz, M., et al. (2013), A decade of Predictions in Ungauged Basins (PUB) a review, *Hydrol. Sci. J.*, *58*(6), 1198–1255.

Huete, A., K. Didan, T. Miura, E. P. Rodriguez, X. Gao, and L. G. Ferreira (2002), Overview of the radiometric and biophysical performance of the MODIS vegetation indices, *Remote Sens. Environ.*, *83*(1–2), 195–213.

Impens, I., and R. Lemeur (1969), Extinction of net radiation in different crop canopies, *Theor. Appl. Climatol.*, *17*(4), 403–412.

International Panel on Climate Change (2001), *Climate Change 2001: The Scientific Basis: Contribution of Working Group I to the Third Assessment Report of the International Panel on Climate Change*, edited by J. T. Houghton et al., Cambridge Univ. Press, Cambridge, U. K., and New York.

Jung, M., M. Reichstein, and A. Bondeau (2009), Towards global empirical upscaling of FLUXNET eddy covariance observations: Validation of a model tree ensemble approach using a biosphere model, *Biogeosciences*, *6*(10), 2001–2013.

Jung, M., et al. (2010), Recent decline in the global land evapotranspiration trend due to limited moisture supply, *Nature*, *467*(7318), 951–954.

Jung, M., et al. (2011), Global patterns of land-atmosphere fluxes of carbon dioxide, latent heat, and sensible heat derived from eddy cov-ariance, satellite, and meteorological observations, *J. Geophys. Res.*, *116*, G00J07, doi:10.1029/2010JG001566.

Kamakura, M., Y. Kosugi, S. Takanashi, K. Matsumoto, M. Okumura, and E. Philip (2011), Patchy stomatal behavior during midday depression of leaf CO2 exchange in tropical trees, *Tree Physiol.*, *31*(2), 160–168.

Keane, R. E., K. C. Ryan, T. T. Veblen, C. D. Allen, J. Logan, and B. Hawkes (2002), Cascading effects of fire exclusion in the Rocky Mountain ecosystems: A literature review. USDA Forest Service, Rocky Mountain Research Station, General Technical Report RMRS-GTR-91, 24 pp.

Legates, D. R., and G. J. McCabe (1999), Evaluating the use of "goodness-of-fit" measures in hydrologic and hydroclimatic model validation, *Water Resour. Res.*, *35*(1), 233–241, doi:10.1029/1998WR900018.

Li, X., et al. (2009), Watershed allied telemetry experimental research, *J. Geophys. Res.*, *114*, D22103, doi:10.1029/2008JD011590.

Liu, S. M., Z. W. Xu, W. Z. Wang, Z. Z. Jia, M. J. Zhu, J. Bai, and J. M. Wang (2011), A comparison of eddy-covariance and large aperture scin-tillometer measurements with respect to the energy balance closure problem, *Hydrol. Earth Syst. Sci.*, *15*(4), 1291–1306.

Mallick, K., A. Jarvis, J. B. Fisher, K. P. Tu, E. Boegh, and D. Niyogi (2013), Latent heat flux and canopy conductance based on Penman-Monteith, Priestley-Taylor equation, and Bouchet's complementary hypothesis, *J. Hydrometeorol.*, *14*(2), 419–442.

McCabe, M. F., A. Ershadi, C. Jimenez, D. G. Miralles, D. Michel, and E. F. Wood (2016), The GEWEX LandFlux project: Evaluation of model evaporation using tower-based and globally gridded forcing data, *Geosci. Model. Dev.*, *9*(1), 283–305.

McKay, M. D. (1988), in *Sensitivity and Uncertainty Analysis Using a Statistical Sample of Input Values*, edited by Y. Ronen, pp. 145–186 , CRC Press, Inc., Boca Raton, Fla.

Meyer, W. S., E. Kondrlova, and G. R. Koerber (2015), Evaporation of perennial semi-arid woodland in southeastern Australia is adapted for irregular but common dry periods, *Hydrol. Process.*, *29*(17), 3714–3726.

Michel, D., et al. (2016), The WACMOS-ET project—Part 1: Tower-scale evaluation of four remote-sensing-based evapotranspiration algo-rithms, *Hydrol. Earth Syst. Sci.*, *20*(2), 803–822.

Monteith, J. L. (1965), Evaporation and environment, in *The State and Movement of Water in Living Organisms, Symposium of the Society of Experimental Biology*, pp. 205–234 , Cambridge Univ. Press, Cambridge.

Moreno, L., F. Martin, M. L. Munoz, and S. Garrido (2016), Differential evolution Markov chain filter for global localization, *J. Intell. Robot Syst.*, *82*(3–4), 513–536.

Moriasi, D. N., J. G. Arnold, M. W. Van Liew, R. L. Bingner, R. D. Harmel, and T. L. Veith (2007), Model evaluation guidelines for systematic quantification of accuracy in watershed simulations, *T Asabe*, *50*(3), 885–900.

Moussa, R., and N. Chahinian (2009), Comparison of different multi-objective calibration criteria using a conceptual rainfall-runoff model of flood events, *Hydrol. Earth Syst. Sci.*, *13*(4), 519–535.

Mu, Q. Z., M. S. Zhao, and S. W. Running (2011), Improvements to a MODIS global terrestrial evapotranspiration algorithm, *Remote Sens. Environ.*, *115*(8), 1781–1800.

Mu, Q., F. A. Heinsch, M. Zhao, and S. W. Running (2007), Development of a global evapotranspiration algorithm based on MODIS and global meteorology data, *Remote Sens. Environ.*, *111*(4), 519–536.

Nash, J. E., and J. V. Sutcliffe (1970), River flow forecasting through conceptual models part I-A discussion of principles, *J. Hydrol.*, *10*(3), 282–290.

Norman, J. M., W. P. Kustas, and K. S. Humes (1995), Source approach for estimating soil and vegetation energy fluxes in observations of directional radiometric surface-temperature, *Agric. For. Meteorol.*, *77*(3–4), 263–293.

Nossent, J., P. Elsen, and W. Bauwens (2011), Sobol' sensitivity analysis of a complex environmental model, *Environ. Modell. Software*, *26*(12), 1515–1525.

Oki, T., and S. Kanae (2006), Global hydrological cycles and world water resources, *Science*, *313*(5790), 1068–1072.

Osidele, O. O., and M. B. Beck (2001), Identification of model structure for aquatic ecosystems using regionalized sensitivity analysis, *Water Sci. Technol.*, *43*(7), 271–278.

Pappenberger, F., K. J. Beven, M. Ratto, and P. Matgen (2008), Multi-method global sensitivity analysis of flood inundation models, *Adv. Water Resour.*, *31*(1), 1–14.

Potter, C. S., J. T. Randerson, C. B. Field, P. A. Matson, P. M. Vitousek, H. A. Mooney, and S. A. Klooster (1993), Terrestrial ecosystem production—A process model-based on global satellite and surface data, *Global Biogeochem. Cycles*, *7*(4), 811–841, doi:10.1029/93GB02725.

Price, K., and R. Storn (1997), Differential evolution—A simple evolution strategy for fast optimization, *Dr. Dobb's J.*, *22*(4, 18).

Priestley, C. H. B., and R. J. Taylor (1972), On the assessment of surface heat flux and evaporation using large-scale parameters, *Mon. Weather Rev.*, *100*, 81–92.

Rango, A., and A. I. Shalaby (1998), Operational applications of remote sensing in hydrology: Success, prospects and problems, *Hydrol. Sci. J.*, *43*(6), 947–968.

Raupach, M. R. (2001), Combination theory and equilibrium evaporation, *Q. J. R. Meteorol. Soc.*, *127*(574), 1149–1181.

Roberts, G. O., and J. S. Rosenthal (2001), Optimal scaling for various Metropolis-Hastings algorithms, *Stat. Sci.*, *16*(4), 351–367.

Ross, J. (1976), Radiative transfer in plant communities, in *Vegetation and the atmosphere*, edited by J. L. Monteith, pp. 13–56 , Academic Press, London.

Ryu, Y., et al. (2012), On the temporal upscaling of evapotranspiration from instantaneous remote sensing measurements to 8-day mean daily-sums, *Agric. For. Meteorol.*, *152*, 212–222.

Saltelli, A., S. Tarantola, and F. Campolongo (2000), Sensitivity analysis as an ingredient of modeling, *Stat. Sci.*, *15*(4), 377–395.

Scott, R. L., G. D. Jenerette, D. L. Potts, and T. E. Huxman (2009), Effects of seasonal drought on net carbon dioxide exchange from a woody-plant-encroached semiarid grassland, *J. Geophys. Res.*, *114*, G04004, doi:10.1029/2008JG000900.

Senay, G. B., S. Leake, P. L. Nagler, G. Artan, J. Dickinson, J. T. Cordova, and E. P. Glenn (2011), Estimating basin scale evapotranspiration (ET) by water balance and remote sensing methods, *Hydrol. Process.*, *25*(26), 4037–4049.

Shimizu, T. (2007), Practical applicability of high frequency correction theories to CO2 flux measured by a closed-path system, *Boundary Layer Meteorol.*, *122*(2), 417–438.

Sieber, A., and S. Uhlenbrook (2005), Sensitivity analyses of a distributed catchment model to verify the model structure, *J. Hydrol.*, *310*(1–4), 216–235.

Sobol, I. M. (1990), On sensitivity estimation of nonlinear mathematical models, *Matem. Mod.*, *2*(1), 112–118.

Sobol, I. M. (2001), Global sensitivity indices for nonlinear mathematical models and their Monte Carlo estimates, *Math Comput. Simul.*, *55*(1–3), 271–280.

Stoy, P. C., et al. (2013), A data-driven analysis of energy balance closure across FLUXNET research sites: The role of landscape scale heterogeneity, *Agric. For. Meteorol.*, *171*, 137–152.

Stoy, P. C., A. M. Trowbridge, and W. L. Bauerle (2014), Controls on seasonal patterns of maximum ecosystem carbon uptake and canopy-scale photosynthetic light response: Contributions from both temperature and photoperiod, *Photosynth. Res.*, *119*(1–2), 49–64.

Su, Z. (2002), The Surface Energy Balance System (SEBS) for estimation of turbulent heat fluxes, *Hydrol. Earth Syst. Sci.*, *6*(1), 85–99.

Tang, Y., P. Reed, T. Wagener, and K. van Werkhoven (2007), Comparing sensitivity analysis methods to advance lumped watershed model identification and evaluation, *Hydrol. Earth Syst. Sci.*, *11*(2), 793–817.

Taylor, K. E. (2001), Summarizing multiple aspects of model performance in a single diagram, *J. Geophys. Res.*, *106*(D7), 7183–7192, doi:10.1029/2000JD900719.

Ter Braak, C. J. F. (2006), A Markov Chain Monte Carlo version of the genetic algorithm differential evolution: Easy Bayesian computing for real parameter spaces, *Stat. Comput.*, *16*(3), 239–249.

Trenberth, K. E., and L. Smith (2009), The three dimensional structure of the atmospheric energy budget: Methodology and evaluation, *Clim. Dynam.*, *32*(7–8), 1065–1079.

Twine, T. E., W. P. Kustas, J. M. Norman, D. R. Cook, P. R. Houser, T. P. Meyers, J. H. Prueger, P. J. Starks, and M. L. Wesely (2000), Correcting eddy-covariance flux underestimates over a grassland, *Agric. For. Meteorol.*, *103*(3), 279–300.

van Werkhoven, K., T. Wagener, P. Reed, and Y. Tang (2008), Characterization of watershed model behavior across a hydroclimatic gradient, *Water Resour. Res.*, *44*, W01429, doi:10.1029/2007WR006271.

Vinukollu, R. K., E. F. Wood, C. R. Ferguson, and J. B. Fisher (2011), Global estimates of evapotranspiration for climate studies using multi-sensor remote sensing data: Evaluation of three process-based approaches, *Remote Sens. Environ.*, *115*(3), 801–823.

Wagener, T., N. McIntyre, M. J. Lees, H. S. Wheater, and H. V. Gupta (2003), Towards reduced uncertainty in conceptual rainfall-runoff modelling: Dynamic identifiability analysis, *Hydrol. Process.*, *17*(2), 455–476.

Wang, K. C., and R. E. Dickinson (2012), A review of global terrestrial evapotranspiration: Observation, modeling, climatology, and climatic variability, *Rev. Geophys.*, *50*, RG2005, doi:10.1029/2011RG000373.

Wang, K. C., R. E. Dickinson, M. Wild, and S. L. Liang (2010), Evidence for decadal variation in global terrestrial evapotranspiration between 1982 and 2002: 1. Model development, *J. Geophys. Res.*, *115*, D20112, doi:10.1029/2009JD013671.

Xue, L. L., and Z. T. Pan (2008), Ensemble calibration and sensitivity study of a surface CO2 flux scheme using an optimization algorithm, *J. Geophys. Res.*, *113*, D10109, doi:10.1029/2007JD009333.

Yang, J. (2011), Convergence and uncertainty analyses in Monte-Carlo based sensitivity analysis, *Environ. Modell. Software*, *26*(4), 444–457.

Yao, Y. J., et al. (2013), MODIS-driven estimation of terrestrial latent heat flux in China based on a modified Priestley-Taylor algorithm, *Agric. For. Meteorol.*, *171*, 187–202.

Yao, Y. J., S. L. Liang, S. H. Zhao, Y. H. Zhang, Q. M. Qin, J. Cheng, K. Jia, X. H. Xie, N. N. Zhang, and M. Liu (2014), Validation and application of the modified satellite-based Priestley-Taylor algorithm for mapping terrestrial evapotranspiration, *Remote Sens-Basel*, *6*(1), 880–904.

Yuan, W. P., et al. (2010), Global estimates of evapotranspiration and gross primary production based on MODIS and global meteorology data, *Remote Sens. Environ.*, *114*(7), 1416–1431.

Zhang, C., J. G. Chu, and G. T. Fu (2013), Sobol's sensitivity analysis for a distributed hydrological model of Yichun River Basin, China, *J. Hydrol.*, *480*, 58–68.

Zhang, Y. G., et al. (2013), Extreme precipitation patterns and reductions of terrestrial ecosystem production across biomes, *J. Geophys. Res. Biogeosci.*, *118*, 148–157, doi:10.1029/2012JG002136.

Zhu, G. F., Y. H. Su, X. Li, K. Zhang, and C. B. Li (2013), Estimating actual evapotranspiration from an alpine grassland on Qinghai-Tibetan plateau using a two-source model and parameter uncertainty analysis by Bayesian approach, *J. Hydrol.*, *476*, 42–51.

Zhu, G. F., X. Li, Y. H. Su, K. Zhang, Y. Bai, J. Z. Ma, C. B. Li, X. L. Hu, and J. H. He (2014), Simultaneously assimilating multivariate data sets into the two-source evapotranspiration model by Bayesian approach: Application to spring maize in an arid region of northwestern China, *Geosci. Model. Dev.*, *7*(4), 1467–1482.

Zhu, G. F., X. Li, K. Zhang, Z. Y. Ding, T. Han, J. Z. Ma, C. L. Huang, J. H. He, and T. Ma (2016), Multi-model ensemble prediction of terrestrial evapotranspiration across north China using Bayesian model averaging, *Hydrol. Process.*, *30*(16), 2861–2879.